CITATION

Mathis, J.T., J.N. Cross, W. Evans, and S.C. Doney. 2015. Ocean acidification in the surface waters of the Pacific-Arctic boundary regions. *Oceanography* 28(2):122–135, http://dx.doi.org/10.5670/oceanog.2015.36.
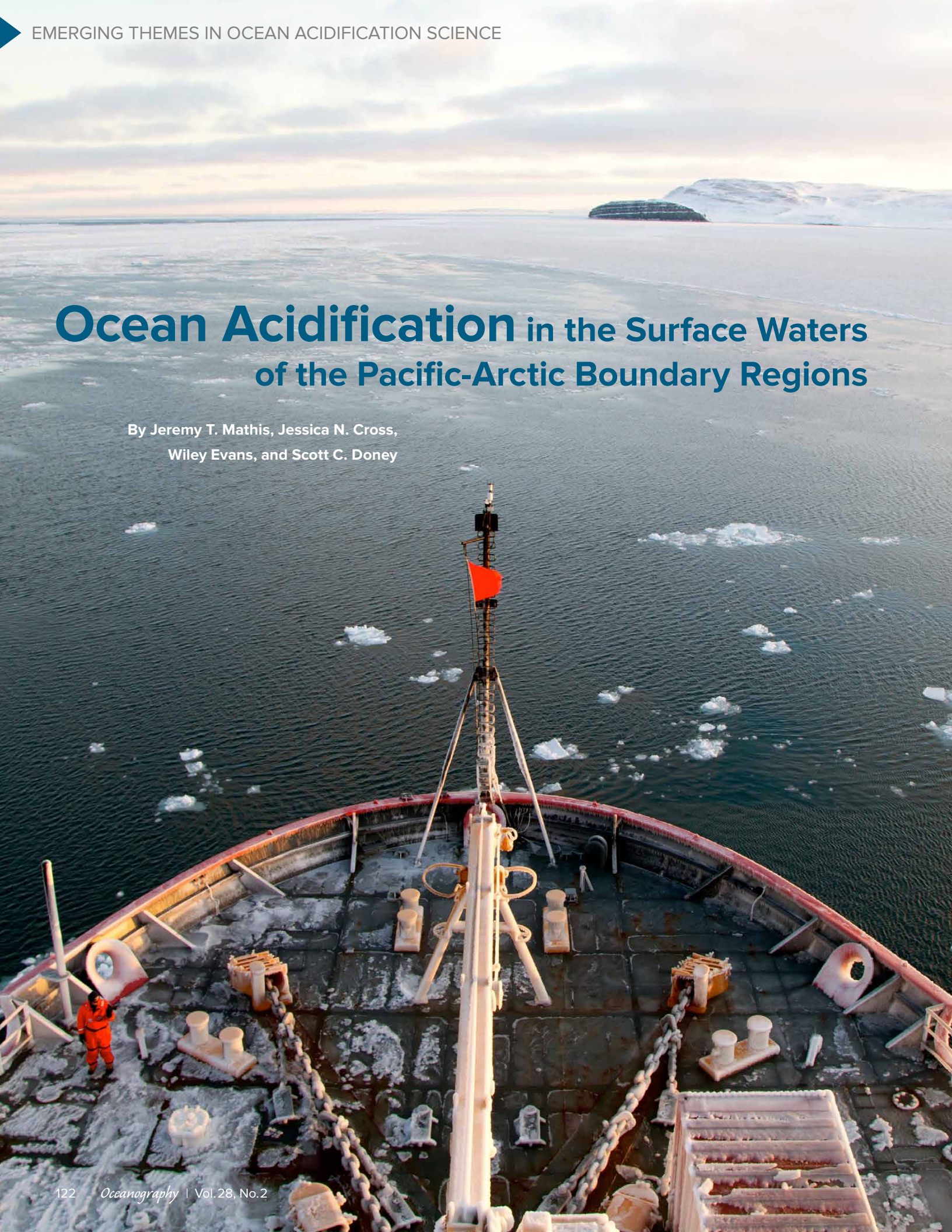
DOI

http://dx.doi.org/10.5670/oceanog.2015.36

Ocean Acidification in the Surface Waters of the Pacific-Arctic Boundary Regions

By Jeremy T. Mathis, Jessica N. Cross, Wiley Evans, and Scott C. Doney

" As Ω_{arag} in these shelf seas slips below the present-day range of large seasonal variability by mid-century, the diverse ecosystems that support some of the largest commercial and subsistence fisheries in the world may be under tremendous pressure. "

ABSTRACT. The continental shelves of the Pacific-Arctic Region (PAR) are especially vulnerable to the effects of ocean acidification (OA) because the intrusion of anthropogenic CO_2 is not the only process that can reduce pH and carbonate mineral saturation states for aragonite (Ω_{arag}). Enhanced sea ice melt, respiration of organic matter, upwelling, and riverine inputs have been shown to exacerbate CO_2-driven ocean acidification in high-latitude regions. Additionally, the indirect effect of changing sea ice coverage is providing a positive feedback to OA as more open water will allow for greater uptake of atmospheric CO_2. Here, we compare model-based outputs from the Community Earth System Model with a subset of recent ship-based observations, and take an initial look at future model projections of surface water Ω_{arag} in the Bering, Chukchi, and Beaufort Seas. We then use the model outputs to define benchmark years when biological impacts are likely to result from reduced Ω_{arag}. Each of the three continental shelf seas in the PAR will become undersaturated with respect to aragonite at approximately 30-year intervals, indicating that aragonite undersaturations gradually progress upstream along the flow path of the waters as they move north from the Pacific Ocean. However, naturally high variability in Ω_{arag} may indicate higher resilience of the Bering Sea ecosystem to these low-Ω_{arag} conditions than the ecosystems of the Chukchi and the Beaufort Seas. Based on our initial results, we have determined that the annual mean for Ω_{arag} will pass below the current range of natural variability in 2025 for the Beaufort Sea and 2027 for the Chukchi Sea. Because of the higher range of natural variability, the annual mean for Ω_{arag} for the Bering Sea does not pass out of the natural variability range until 2044. As Ω_{arag} in these shelf seas slips below the present-day range of large seasonal variability by mid-century, the diverse ecosystems that support some of the largest commercial and subsistence fisheries in the world may be under tremendous pressure.

INTRODUCTION

Over the last few years, ocean acidification (OA) has emerged as one of the most prominent issues in marine research, and it has entered the public consciousness as an existential threat (e.g., Frisch et al., 2015). However, not all regions experience OA at the same level, and regional hotspots have emerged where more pronounced expressions of OA can be observed. This is particularly true in the high-latitude North Pacific and the western Arctic Ocean, where the intensity, duration, and extent of OA events have been greater than in many other ocean basins (e.g., Mathis et al., 2011a; Cross et al., 2013). Given the predictions for the pace of future changes in the Pacific-Arctic Region (PAR), the area is commonly referred to as a bellwether for human-induced changes in carbonate chemistry (Fabry et al., 2009) or the proverbial "canary in the coal mine" for the rest of the global ocean.

OA is a global phenomenon that is driven by oceanic uptake of anthropogenic carbon dioxide (CO_2) from the atmosphere that has been emitted during the Anthropocene and that has accelerated over the last 50–100 years in step with rising global CO_2 emissions. The rapid accumulation of CO_2 in the upper thousand meters of the ocean has fundamentally altered the chemistry of seawater, making the ocean on average ~30% more acidic, while decreasing the saturation states (Ω) of calcium carbonate minerals that are critical for the formation and maintenance of biogenic shells and tests (e.g., Feely et al., 2004, 2009; Sabine et al., 2004; Sabine and Feely, 2007). As carbonate mineral saturations are reduced in the ocean, many marine calcifying organisms struggle to maintain normal physiological functions (e.g., Feely et al., 2009; Cooley and Doney, 2009; Kroeker et al., 2010; Barton et al., 2012; Waldbusser et al., 2014). This issue is critical because one of the most prolific fisheries in the global ocean spans the Bering and Chukchi Seas, where there is a confluence of rapid environmental change and vulnerable commercial and subsistence species (Mathis et al., 2011a; Mathis et al., in press; Long et al., 2013a,b).

The boundary regions over the

continental shelves of the Bering, Chukchi, and Beaufort Seas (Figure 1) are especially vulnerable to the effects of OA because the intrusion of anthropogenic CO_2 is not the only process that can reduce Ω (e.g., Evans et al., 2014; Reisdorph and Mathis, 2014). Natural processes such as seasonal sea ice melt (Yamamoto-Kawai et al., 2009a,b, 2013), respiration of organic matter (Bates and Mathis, 2009), upwelling along the continental shelves (Mathis et al., 2012),

and riverine inputs (Mathis et al., 2011b) can also exacerbate reductions in Ω. Additionally, the indirect effect of changing sea ice coverage is providing a positive feedback to OA. For example, the reduction in Arctic and subArctic sea ice observed in recent years can be attributed to increased warming caused at least in part by rising atmospheric CO_2 levels. The reduction in the extent and duration of sea ice cover leads to longer open water periods, allowing for enhanced upwelling

and changes in the timing and intensity of primary production (Lavoie et al., 2010; Arrigo and van Dijken, 2011) and sea-air gas exchange of CO_2 (Evans and Mathis, 2013; Cross et al., 2014; recent work of authors Evans, Mathis, Cross, and colleagues). Combined with the fact that the continental shelves in this region are already preconditioned to have relatively low Ω compared to the global ocean due to ocean circulation patterns and colder water temperatures (Fabry et al., 2009),
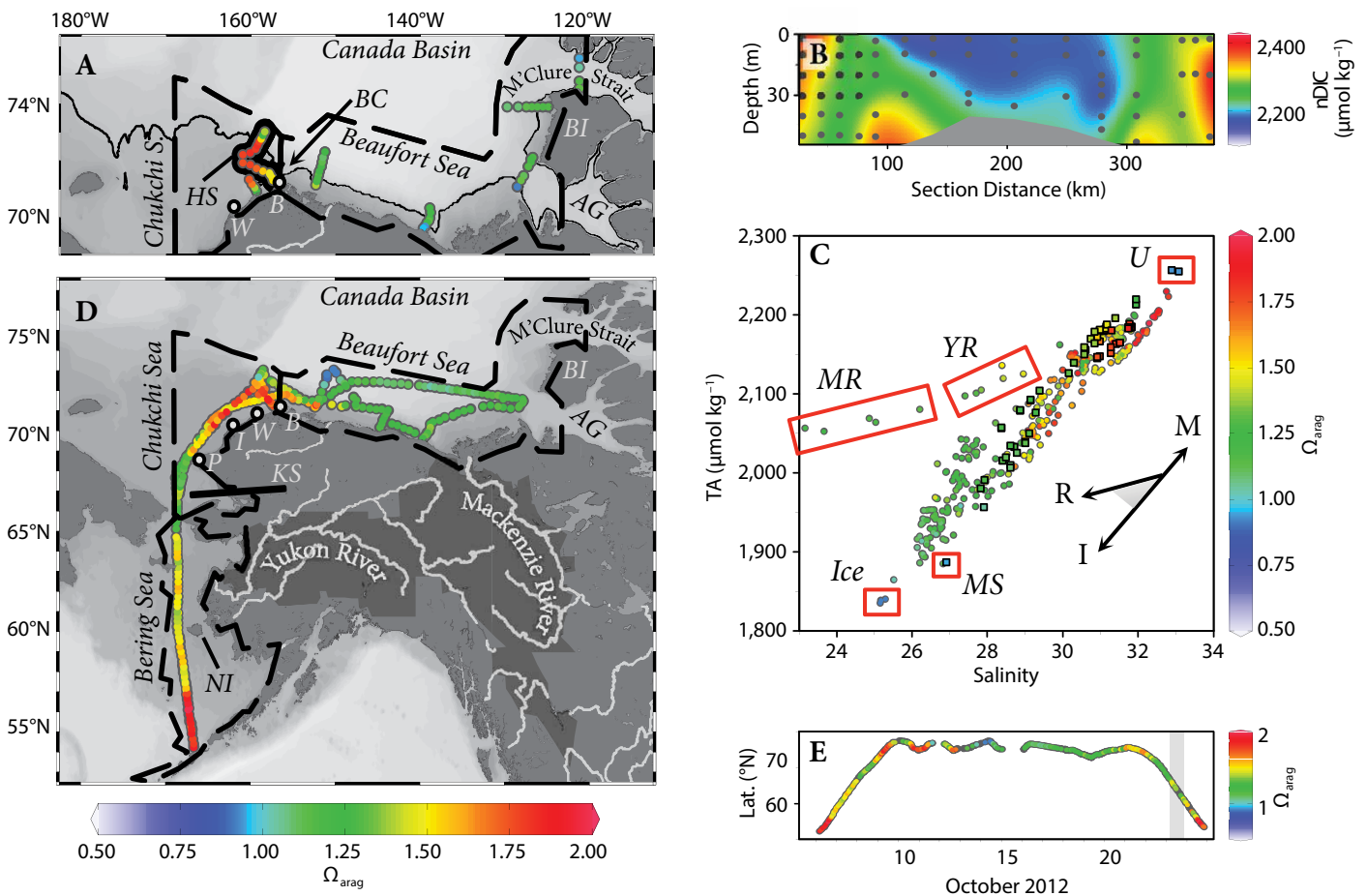

FIGURE 1. (A) Discrete surface water carbonate mineral saturation states from aragonite (Ω_{arag}) data collected during 2011. The boundaries for the Chukchi Sea are indicated by dashed black lines, with the boundary between the Chukchi and Beaufort Seas lying approximately at Point Barrow (*B*). For reference, Amundsen Gulf (*AG*), Wainright (*W*), and Hannah Shoal (*HS*) are also indicated. Barrow Canyon (*BC*) is indicated by an arrow and the 80 m isobathic contour (thin black line). (B) Section plot for the 2011 Chukchi Sea transect (bolded section in panel A) showing salinity-normalized dissolved inorganic carbon concentrations (nDIC) from the shelf break (left edge), over Hannah Shoal (~40 m depth) and across Barrow Canyon toward the coast (right edge). Low nDIC values indicate drawdown of DIC due to primary production; higher values in the subsurface indicate respiration. High surface values can indicate the influences of high-DIC river waters or ice melt. (C) Water mass plot for discrete surface water data collected in 2011 and 2012. The vector diagram indicates increasing fractions of marine water (M), sea ice melt (I), and river water (R). The influence of both the Mackenzie and Yukon Rivers are highlighted (*MR* and *YR*, respectively; see also panel D). Areas of undersaturation are also highlighted in red boxes, including undersaturations from upwelling (*U*; nearshore of section near 140°W in panel A), and ice melt in the Canada basin (*Ice;* see also lowest Ω_{arag} in panel D) and in M'Clure Strait (*MS*; see panel A). (D) Discrete surface water Ω_{arag} data collected during 2012. The boundaries for the shelf seas are indicated by dashed black lines as in panel A, with the boundary between the Bering and Chukchi Seas denoted at Bering Strait. For reference, Nunivak Island (NI), Kotzebue Sound (KS), Point Hope (P), Icy Cape (I), Wainright (W), Barrow (B), and Amundsen Gulf (AG) are also indicated. (E) Underway track of discrete surface data collected during 2012. Ω_{arag} was slightly lower on the return transit through the central Bering Sea due to an increased freshwater fraction, indicated by the gray shading.

these direct and indirect acidification processes make the region highly vulnerable to further reductions in seawater pH and Ω (Steinacher et al., 2009), with unknown, but likely detrimental, consequences for the marine food web. Therefore, it is imperative to quantify the current extent of OA across the region and project the future intensity of OA events.

BACKGROUND

High-latitude ocean waters, like those around Alaska (Figure 1), have naturally low carbonate (CO_3^{2-}) concentrations (Fabry et al., 2009) and are thus considered to be more vulnerable to the impacts of OA on shorter time scales. In low CO_3^{2-} areas, additional losses of CO_3^{2-} from OA represent a much greater proportional change to the system. Waters circulating along the coastline of Alaska are derived from CO_2-rich waters that are upwelled in the North Pacific, where anthropogenically induced pH changes have already been directly observed (Byrne et al., 2010). As these waters flow northward, eventually into the Bering Sea and the Arctic Ocean, low sea surface temperature and increased solubility of CO_2 favor naturally low CO_3^{2-} surface concentrations (Key et al., 2004; Orr et al., 2005; Orr, 2011).

The primary mechanism controlling carbonate chemistry in the Bering Sea is the biological pump (Mathis et al., 2011a,b; Cross et al., 2012). Biological production decreases the partial pressure of CO_2 (pCO_2) at the surface (Bates et al., 2011; Cross et al., 2014) and increases Ω in summer (Mathis et al., 2011b). The pCO_2 can range from 150–400 µatm in the surface mixed layer, while the saturation state for aragonite (Ω_{arag}), the more soluble of the two most common biogenic calcium carbonate structures, oscillates between an annual maximum of 3.5 and a minimum of 0.8. To date, the only surface locations where aragonite has been observed to be undersaturated ($\Omega < 1.0$) were where sea ice melt or river runoff predominated, both of which are low in total alkalinity (TA) relative to

marine waters (Mathis et al., 2011b).

Farther north, in the western Arctic Ocean (Figure 1), reductions in sea ice coverage and thickness (e.g., Stroeve et al., 2007) have been especially pronounced in the Chukchi Sea and adjacent Canada Basin, with implications for surface layer carbonate mineral suppression. In the past decade, ice-free periods have lengthened by several days each year, and open water areas have substantially increased, particularly in autumn months (Stroeve et al., 2007; Comiso et al., 2008). This melt has been substantial enough to freshen the surface throughout the Canada Basin (Yamamoto-Kawai et al., 2009a), and has been shown to lower Ω, producing corrosive conditions in surface waters in some areas (Yamamoto-Kawai et al., 2009b; Mathis et al., 2011a; Cross et al., 2013; Bates et al., 2014).

Unlike the Chukchi and Bering Seas, the Beaufort Sea shelf (Figure 1) is relatively narrow, and it has a limited physical supply of nutrients (e.g., Carmack and Wassmann, 2006). Rates of phytoplankton primary production over the shelf have been estimated at ~ 6–12 g C m^{-2} yr^{-1} (Anderson and Kaltin, 2001; Macdonald et al., 2010), compared to ≥ 300 g C m^2 yr^{-1} in the Chukchi Sea (i.e., Mathis et al., 2009; Macdonald et al., 2010). The primary natural process contributing to corrosive events in the Beaufort Sea is upwelling of halocline waters from the Canada Basin (Mathis et al., 2012) that are formed on the Chukchi shelf and then exported into the deep Arctic Ocean (Mathis et al., 2007; Kadko et al., 2008). During an observed upwelling event in the Beaufort Sea, upper halocline water replete in CO_2 and undersaturated in aragonite reached the surface and moved all the way inshore along the Beaufort shelf, covering thousands of square kilometers (Mathis et al., 2012). Although some level of storm-driven upwelling is typical in this region, especially in autumn, land-fast as well as pack ice has historically returned before major late-autumn storm systems begin to pass through the region. In recent years, the western Arctic

has seen an unprecedented loss of both sea ice extent and volume (Stroeve et al., 2007), resulting in sea-ice-free conditions through the annual peak in storm frequency and intensity (September to October). In the future, the Beaufort shelf is likely to be persistently, if not continually, exposed to waters that are undersaturated with respect to aragonite as sea ice cover continues to diminish under warming conditions (Mathis et al., 2012).

The future of OA events and biogeochemistry over these continental shelf seas will be a complex interaction of competing mechanisms and feedbacks on ocean pH resulting from the multiple impacts of a rapidly changing environment. Warming temperatures may cause increasing freshwater discharges (Peterson et al., 2002) and melting of permafrost, leading to release of larger amounts of terrestrial organic matter into coastal regions and augmenting CO_2 accumulation from respiration processes (e.g., Striegl et al., 2007; Walvoord and Striegl, 2007; Garneau et al., 2009). Increased sea ice losses will contribute waters low in total alkalinity and undersaturated in aragonite to the ocean surface (Bates et al., 2014), permit greater upwelling (Mathis et al., 2012), and may fundamentally change the timing and fate of primary production in both the Bering and Chukchi Seas (Arrigo et al., 2008; Cai et al., 2010; Hunt et al., 2011; Stabeno et al., 2012a,b). If primary production increases due to increased light availability and a longer effective growing season, it could promote enhanced rates of sea-air exchange of CO_2 and increased influxes of anthropogenic CO_2 into the surface waters (e.g., Arrigo et al., 2008; recent work of authors Evans, Mathis, Cross, and colleagues). However, stratification from melting sea ice and increased freshwater inflows may reduce nutrient availability at the surface and lower primary production, leading to reduced uptake rates of anthropogenic CO_2 in some areas (Cai et al., 2010; Roy et al., 2011). By contrast, reduced spatial ice coverage in autumn could also permit

increased efflux of CO_2 back into the atmosphere, lowering seawater pCO_2 and increasing pH. Increasing sea surface temperatures will further modify these rates of exchange. Given this complex set of both positive and negative feedbacks to OA, it is difficult to predict how this region will respond.

Many global-scale model studies indicate that the largest and most rapid changes in pH will occur in the Arctic Ocean and the Bering Sea. For example, persistent aragonite undersaturations in surface waters have been projected to occur within the next decade for at least 10% of the Arctic Ocean (Steinacher et al., 2009). In the Bering Sea, some calcite undersaturations have already been observed (Mathis et al., 2011b; Cross et al., 2013), and they are projected to emerge in the Arctic by the end of the century (Feely et al., 2009). These rates of change are much faster than any time in the past 50 million years (Caldeira and Wickett, 2003; Hönisch et al., 2012). While OA will likely create winning and losing ecological scenarios for different groups, vulnerable species may suffer from higher energy costs as they are forced to acclimate to increasingly acidic conditions. The expected pace and magnitude of change in carbonate chemistry could also limit the capacity for evolutionary adaptation processes (Barry et al., 2011). Species with relatively small populations and long generation times (e.g., fish) are expected to have the lowest potential for adaptation, as selection for tolerant genotypes is limited to just a few generations (Willi et al., 2006; Bell and Gonzalez, 2009; Fabry et al., 2009; Hoffman and Sgrò, 2011; Bernhardt and Leslie, 2013).

Given the complexity in the physical and biogeochemical drivers that are affecting carbonate mineral saturations states, it is imperative to study these processes using multiple tools and over varying temporal and spatial scales. Here, we compare time-matched model outputs with a subset of recent ship-based data to illustrate the fine-scale variability.

We then use the model projections of Ω_{arag} for surface waters to more broadly explore benchmark years when biological impacts are likely to result from reduced Ω_{arag} for each shelf sea. One biogeochemical threshold is the saturation horizon, or the year at which the annual average value of Ω_{arag} falls below 1.0, favoring the dissolution of carbonate minerals. Biological impacts can also result when organisms are exposed to conditions outside the range of variability in their natural habitat, and we estimate the year at which the annual average value of Ω_{arag} falls outside the variability observed in present conditions (Cooley et al., 2012). This first approximation in defining these benchmarks for biological stress clearly shows the pace of change in the Arctic, and it highlights the potential of focused modeling efforts and integrated studies for refining projections of future change in the Pacific Arctic Region.

METHODS
Data Collection and Analysis
Direct observations of temperature, salinity, TA, and dissolved inorganic carbon (DIC) were made using surface samples collected on a USCGC *Healy* cruise track through the Bering, Chukchi, and Beaufort Seas in both October of 2011 and October of 2012 (Figure 1). In 2011, these samples were collected using a Sea-Bird 911+ conductivity-temperature-depth (CTD) instrument mounted on a 24-position 10-liter rosette. In 2012, the samples were made using a SBE45 sensor coupled to a pumped underway seawater system. During each cruise, seawater samples for DIC/TA were drawn into pre-cleaned 300 mL borosilicate bottles. These samples were immediately poisoned with 200 µL of saturated mercuric chloride ($HgCl_2$) to halt biological activity.

In 2011, DIC and TA samples were analyzed with a highly precise and accurate gas extraction/coulometric detection system using a VINDTA 3C coupled to a CO_2 coulometer (model 5012; UIC Coulometrics). In 2012, a VINDTA 3S system was used for the titration of TA

samples. DIC was determined using a high precision (<0.05% CVV) small-volume DIC infrared-based instrument (AIRICA, Automated Infra-Red Inorganic Carbon Analyzer, coupled to a LI-COR LI-7000 CO_2/H_2O Analyzer), as in Bates et al. (2014). The VINDTA 3C, 3S, and AIRICA systems are all manufactured by MARIANDA (L. Mintrop, http://marianda.com). Routine analyses of Certified Reference Materials (CRMs, provided by A.G. Dickson, Scripps Institute of Oceanography) ensured that the accuracy of the DIC and TA measurements were stable over time and within 0.2% (<5 umol kg^{-1}) using the VINDTA 3C and 3S and 0.1% (<3 umol kg^{-1}) using the AIRICA. Seawater pCO_2 and Ω_{arag} were calculated from DIC, TA, temperature, and salinity data using the thermodynamic model of Lewis and Wallace (1995), the carbonic dissociation constants of Mehrbach et al. (1973) as refit by Dickson and Millero (1987), the CO_2 solubility equations of Weiss (1974), and dissociation constants for borate (Dickson, 1990), silicate, and phosphate (Dickson and Goyet, 1994). Uncertainty in the calculation of Ω is ~0.02.

Model Outputs
We projected future chemical properties of the waters of the PAR using outputs from the coupled climate-ocean Community Earth System Model, with a biogeochemistry module enabled (CESM1[BGC]; Keppel-Aleks et al., 2013; Long et al., 2013; Lindsay et al., 2014). The future simulation followed the high-emissions representative concentration pathway (RCP) 8.5 atmospheric CO_2 scenario from the Intergovernmental Panel on Climate Change (van Vuuren et al., 2011), which accounts for future changes in present trends, such as increasing warming and emissions of anthropogenic CO_2. The RCP scenarios show broadly similar atmospheric CO_2 trajectories for the next several decades and only diverge substantially after mid-century. In addition to temperature

increases and CO_2 accumulation, the modeled atmosphere, riverine, ocean and sea ice physics, primary production, and respiration processes in the BGC module should capture changes in freshening and the biological pump. In order to compare these modeled Ω_{arag} with the observations described above, we used a monthly output for October 2011 and 2012, in addition to an annual average output for 2011, 2012, 2050, and 2100. Note that because the fully coupled CESM1 has its own intrinsic climate variability, we cannot directly compare specific model and observational years; instead, our focus is on mean spatial patterns and long-term temporal trends.

RESULTS
Discrete Data

In 2011, data were collected along six hydrographic transect lines covering the eastern Chukchi Sea and Beaufort Sea from approximately Hannah Shoal to M'Clure Strait (Figure 1A). No samples were collected in the Bering Sea during 2011. During this cruise, most surface waters were supersaturated with respect to aragonite. The highest surface Ω_{arag} was found across the eastern Chukchi Sea shelf. Relative to the shelf break and near the coast, depletion of both surface salinity-normalized DIC ($\sim$100 umol kg^{-1}; Figure 1B, bolded section from Figure 1A) and silicate ($\sim$30 umol kg^{-1}; not shown) were apparent over the shallow, well-mixed Hannah Shoal (100–300 km, Figure 1B; *HS*, Figure 1A). The drawdown of these two parameters indicated the persistent influence of primary production processes on surface waters through the month of October. By contrast, both parameters were elevated in bottom waters near the shelf break and across Barrow Canyon (Figure 1B; *BC*, Figure 1A), likely indicating the influences of respiration processes in these deeper areas (Mathis and Questel, 2013).

Surface water aragonite undersaturations in 2011 were observed in conjunction with high fractions of different water masses. Figure 1C shows the

relationship between total alkalinity and salinity during 2011 (shaded squares) and 2012 (shaded circles), with Ω_{arag} shown in color. The vector diagram highlights the mixing between three different water masses in this area: river water (R; low salinity, moderate alkalinity); ice melt (I; low salinity, low alkalinity); and marine waters (M; high salinity, high alkalinity).

In 2011, undersaturations (cool colors) were observed at the marine and ice melt extremes of the data set. The undersaturated marine waters were found along the hydrographic transect just west of the Mackenzie River outflow (Figure 1A, near 140°W, most nearshore stations; *U*, Figure 1C), in conjunction with a previously described upwelling event (Mathis et al., 2012). Here, persistent upwelling-favorable winds transported Arctic Ocean halocline water supersaturated with respect to atmospheric CO_2 and undersaturated in aragonite onto the Beaufort Sea shelf (Mathis et al., 2012). In 2011, the ice-melt-related undersaturations occurred along the north side of M'Clure Strait (Figure 1A, section near 120°W; *MS*, Figure 1C), coinciding with the highest fraction of meltwaters observed during this year.

During 2012, discrete sampling along many of the same lines as 2011 (Figure 1D) and underway sampling along the entire cruise track (Figure 1D,E) permitted collection of nearly six times as many samples as during the previous

year, although the three transects near Amundsen Gulf (*AG*, Figure 1A,D), Banks Island (*BI*, Figure 1A,D) and M'Clure Strait were not reoccupied. At the start of October, Ω_{arag} was relatively high over the southern outer shelf of the Bering Sea (i.e., 100–250 m total water depth). Upon crossing a well-known frontal structure at the 100 m isobath (e.g., Coachman, 1986), Ω_{arag} dropped quickly by $\sim$0.2. Through the central and northern Bering Sea, Ω_{arag} averaged $\sim$1.5. On the return transit through the Bering Sea three weeks later, slight cooling and a small plume of river water discharge were apparent, including slightly lower Ω_{arag} north of Nunivak Island (*NI*, Figure 1D; *YR*, Figure 1D; shaded area, Figure 1E). Values for pCO$_2$ on the return transect were similar to those on the forward transect, indicating a balance between primary production, respiration, and sea-air gas exchange. Through Bering Strait and outside Kotzebue Sound, Ω_{arag} averaged $\sim$1.25. Over the Chukchi Sea shelf north of Icy Cape and Wainright, Ω_{arag} was relatively higher, and it was lower through the entire Beaufort Sea shelf from Point Barrow east to Amundsen Gulf. As in 2011, surface waters undersaturated in aragonite were observed in an area of high sea ice melt concentration in the Canada Basin at $\sim$150°W (*Ice,* Figure 1C; 150°W, Figure 1D; October 14, Figure 1E). Some ice melt was evident over the entire Beaufort Sea shelf west of 149°W.

Mackenzie River water was observed at the easternmost stations in the Beaufort Sea (~130°W) near Amundsen Gulf (*AG*, Figure 1D), although these samples were not found to be undersaturated with respect to aragonite.

Model Output

The color background in Figure 2A,B shows the monthly CESM1(BGC) output for October 1 in 2011 and 2012, respectively, on a 1° latitude by 1° longitude grid. Little small-scale variation is apparent, with most of the Bering Sea being strongly supersaturated in aragonite. The Chukchi Sea was moderately supersaturated, with some areas of higher Ω_{arag} near the coast. In the eastern Beaufort Sea, Ω_{arag} was broadly undersaturated north of the Mackenzie River and near Banks Island. Figure 2C shows the monthly cycle of Ω_{arag} in 2012 for each grid cell in all three seas. During the winter months, Ω_{arag} is lower and much less spatially variable. During the early summer (i.e., June and July), maximum and minimum Ω_{arag} rose, while during late summer (August and September), the monthly minimum Ω_{arag} was drawn down to winter levels and the monthly maximum remained at the annual peak. As a result, the range of Ω_{arag} peaked during late summer and began to decline during October. This cycle is likely indicative of primary production acting in conjunction with circulation processes.

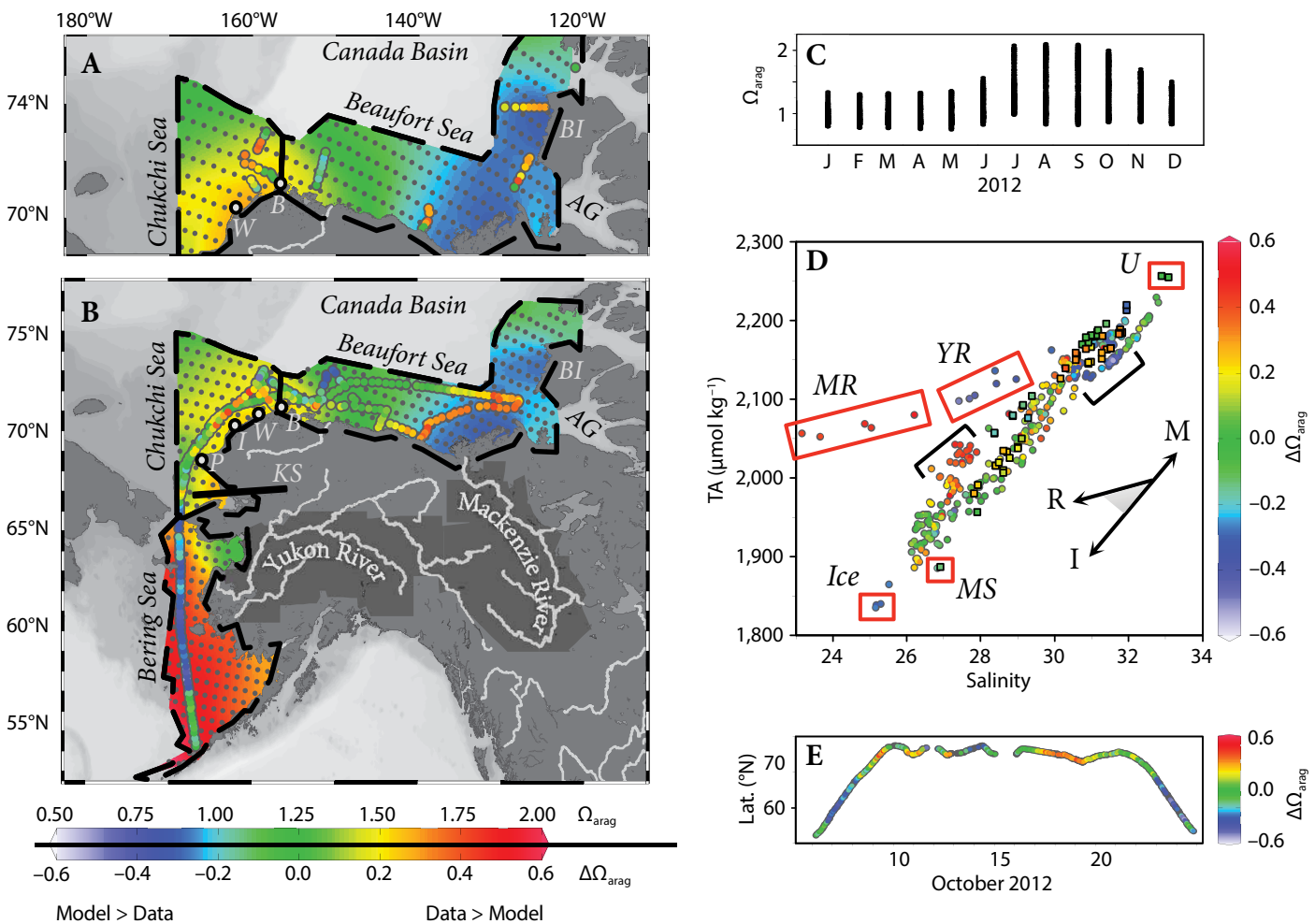For comparison, the difference between our discrete data and the model output is shown overlaid

FIGURE 2. (A) Model output for surface Ω_{arag} for October 1, 2011 (color shading), and difference between the model output and 2011 discrete Ω_{arag} ($\Delta\Omega_{arag}$ = Data – Model; colored dots). Cool colors indicate model Ω_{arag} was higher than the discrete Ω_{arag}, and warm colors indicate the model Ω_{arag} was lower than the discrete Ω_{arag}. Abbreviations are given as in Figure 1A. (B) Model output for surface Ω_{arag} for October 1, 2012 (color shading), and difference between the model and 2012 discrete Ω_{arag} ($\Delta\Omega_{arag}$ = Data – Model; colored dots). Abbreviations are given as in Figure 1D. (C) Monthly range of Ω_{arag} during 2012. While the maximum monthly Ω_{arag} increases during summer, there is very little change in the monthly minimum throughout the year. (D) Water mass plot for discrete surface water data collected in 2011 and 2012, with difference between the model Ω_{arag} and the discrete Ω_{arag} shown in color ($\Delta\Omega_{arag}$ = Data – Model). Strong deviation between the model and the data were found in both the Mackenzie (*MR*) and Yukon (*YR*) Rivers, even at moderate concentrations (indicated by brackets) and high ice melt concentrations (*Ice*). Ω_{arag} in moderate ice melt concentrations (e.g., *MS*) showed good agreement. Coincidental agreement may have been found in upwelled waters (*U*), where the model exhibited low Ω_{arag} due to overprioritized river discharge. (E) Underway track of discrete surface data collected during 2012, with the deviation between the model Ω_{arag} and discrete Ω_{arag} shown in color.

on the model output in Figure 2A,B ($\Delta\Omega_{arag}$ = Data – Model), and in color in Figure 2D,E. Because the model displays a monthly average set of data and low-resolution physical features, these differences highlight many of the small-scale features observed in the discrete data set. For example, differences between the model and the discrete data were high in the areas of active primary production in 2011 (Figures 1A and 2A), in the clear frontal boundary in the southeastern Bering Sea in 2012, and in high concentrations of ice melt in isolated areas, like those observed northwest of Barrow (B, Figure 2A,B) in 2012 (Ice, Figures 1C and 2D).

However, the differences between our observations and the model (Figure 2E) are very small in areas where ice melt concentrations were more moderate (e.g., central Beaufort Sea in 2011 and 2012, and on the north side of M'Clure Strait in 2011). In these areas, the low ice melt concentrations likely indicate that the meltwaters had mixed with surface marine waters over time. Because the model output has a similar time scale to the length of the mixing process that dilutes the ice melt signal, good agreement observed in these well-mixed areas may indicate that the model is capturing this average ice melt signal very well.

The model output and our observations also agreed well in areas where we observed aragonite undersaturation due to upwelling in 2011, although this may be coincidental. The model output predicted large swaths of undersaturation in this area and does not agree well with the surrounding data. One explanation may be that the undersaturations in this area are produced by badly modeled river discharge rather than correctly modeled and widespread upwelling events. The regions of greatest difference between the model output and our data are found in regions influenced by the Mackenzie and Yukon Rivers (color shading, Figure 2B,D). The model projects much lower Ω_{arag} and salinities in the Beaufort Sea, in conjunction with the Mackenzie River end members (MR, Figure 2D), and it projects much higher Ω_{arag} and salinities in the Bering Sea outflow along the Yukon River end members (YR, Figure 2D). This also occurs in areas geographically close to where we observed freshwater discharge, but where we observed that the shelf water end-member dominated (see brackets, Figure 2D; cool colors in the Bering Sea near the Yukon River, Figure 2B; warm colors in the eastern Beaufort Sea near the Mackenzie River, Figure 2A).

DISCUSSION

In comparing our discrete data and the model projections, it is apparent that the model does not reproduce fine-scale variability in areas where freshwater discharge dominates (Figure 2B). This likely results both from the way that the end-member concentrations of DIC and TA are modeled and the volumetric outputs for the Yukon and Mackenzie Rivers. In the CESM1(BGC) simulation, all river inputs are pure freshwater with zero dissolved inorganic carbon and alkalinity concentrations. Pure freshwater has a much lower buffering capacity than seawater or river water, meaning that the impact of the modeled freshwater discharge is likely higher for both rivers than in reality. Our discrete data indicate that the real end members for each river are similar to each other, so the impact of this end-member effect is likely similar in both river basins.

The volumetric effect is likely the cause of the opposite deviations in Ω_{arag} between the model outputs and our discrete data for the Yukon (Data > Model) and Mackenzie (Model > Data) Rivers. Adding pure freshwater dramatically reduces the naturally higher buffering capacity of seawater, which will eventually result in undersaturation despite low $p\text{CO}_2$ (see also Evans et al., 2013). In the Yukon, CESM does not add enough freshwater to the system as would be required to accurately reproduce the effect of river discharge we observed, causing the model to overestimate saturation states through the central Bering Sea (Figure 2B). In the Mackenzie, the model seems to be adding too much freshwater, producing the broad swaths of undersaturation in the eastern Beaufort Sea (Figure 2A,B). Other studies also show that wintertime flows are strongly overestimated in CESM for Arctic rivers with large concentrations of permafrost in the river basins, like the Mackenzie (e.g., Lee et al., 2014).

Outside of the river water issue, the model outputs and discrete measurements agree very well over larger spatial and temporal scales (Table 1). By averaging all of the data that we collected for each shelf sea, we effectively dealt with the fine-scale variations over the size of the shelf sea and the duration of the measurements collected (the 2011 and 2012 cruises both lasted approximately one month), resulting in a product of similar time scale to the monthly model output. While the model covers more spatial area than our discrete observations, a statistical difference between the average shelf sea Ω_{arag} of the two data sets was only observed in the Bering Sea. This likely resulted from the dominance of the river-related deviations over most of the discrete data. We did not find any statistical difference between the average Ω_{arag} for the Chukchi and Beaufort Seas. The minimum Ω_{arag} observed in each shelf sea also agreed well between the model output and the discrete data. The average Ω_{arag} for the data set as a whole was also similar for both the discrete data and the model outputs, with a slightly higher standard deviation in the model output.

Because of this data-model agreement, it is reasonable to assume that the model does present an accurate representation of the present average Ω_{arag} as long as the appropriate scales are considered, and that the model provides an acceptable starting point for projecting future change for these continental shelves. There are also a number of advantages to using the model to project future change, while relying on the discrete data to monitor the present state of the environment and to observe ongoing trends. First, sea ice and extreme conditions make

ship-based and autonomous sampling in the Arctic both logistically and financially challenging, and existing data sets are both spatially and temporally limited. These data also have strong seasonal biases in addition to spatial limitations, including seasonal influences of ice melt, river discharge, and primary production, as already discussed. While the model may not capture exact temporal variability, the seasonal cycle indicated by the monthly model outputs is reasonable; Ω_{arag} are highest in summer months, with the seasonal onset of primary production

and other influences, and winter Ω_{arag} are lower and less variable (Figure 2C).

Second, a numerical simulation also presents a much more robust description of the future than a strictly data-based extrapolation, which we considered. The RCP emission scenarios used by the Earth system models in the IPCC assessments allow the ocean uptake rates of anthropogenic CO_2 to be estimated for a wide range of future atmospheric CO_2 trajectories associated with different human behaviors (i.e., technology, economics, demography, and policy). By contrast,

using the presently observable increase in anthropogenic CO_2 from discrete time-series measurements only allows for an extrapolation in time, effectively assuming a linear extension of present-day atmospheric and ocean trends. Third, the coupled biogeochemical package within the model allows for oceanic and atmospheric disequilibrium in CO_2 concentrations, creating an appropriate lag between emissions and oceanic uptake and using ocean and sea ice physics and biogeochemical processes to influence the rate of oceanic uptake. A data-based approach assumes that all anthropogenic emissions are immediately taken up by the ocean, and can overestimate the rate of anthropogenic CO_2 accumulation and decreases in Ω (Orr et al., 2005).

Figure 3 gives the projected downward trend in the average annual aragonite saturation state for the model output for each shelf region (cool colors) and for all three of these PAR shelf seas taken together, with the saturation horizon shown as a horizontal black line. According to the model outputs, the annual average saturation state for the Beaufort Sea likely crossed the saturation horizon in 2001, meaning that the spatially averaged saturation state for the Beaufort Sea is undersaturated most of the year. The Chukchi Sea is projected to cross this threshold in 2033, with the Bering Sea following another 30 years later. Figure 4 shows the annual average model simulations for 2012, 2050, and 2100. At present, the simulated Bering and Chukchi Seas are both supersaturated with respect to aragonite (warm colors), with the Beaufort Sea weakly undersaturated (cool colors). However, by 2050, the Chukchi Sea is largely undersaturated and the Beaufort Sea is strongly undersaturated, with only weak supersaturations evident in the Bering Sea. By 2100, these undersaturations have progressed southward to cover all PAR surface waters in the model simulation. However, the $\Omega = 1.0$ threshold may not be the best estimate of when the declining saturation state will begin to have an impact on shelf ecosystems.

TABLE 1. Comparison of the average carbonate mineral saturation states for aragonite (Ω_{arag}) for each basin for the discrete data, the October model output, and the annual average model output. The annual average for the model was calculated by averaging each model grid cell temporally and then averaging the entire basin or Pacific-Arctic Region spatially. The first minimum and maximum indicated for the model annual average are the extremes in the annual average simulated for any model grid cell. When the annual average drops below this 2012 minimum, conditions over the entire shelf will be outside the window of present natural spatial variability for most of the year, although the shelfwide average Ω_{arag} may be inside this window during some months (Annual Threshold). The second minimum and maximum listed for the model annual average (indicated by asterisks) are the overall extremes, or the highest and lowest Ω_{arag} value simulated for any model grid cell during any month. When the annual average drops below the 2012 monthly minimum, each shelf sea will experience near-perennial conditions outside the window of present natural spatial and seasonal variability (Persistent Threshold).

		Average			n	Min	Max
BERING SEA	DATA	1.5	±	0.2	75	1.2	2
	MODEL OCTOBER	1.8	±	0.1	112	1.3	2
	MODEL ANNUAL AVERAGE						
	Annual Threshold	1.4	±	0.1	112	1.1	1.5
	Persistent Threshold					0.8	2.1
CHUKCHI SEA	DATA	1.5	±	0.2	143	1	1.9
	MODEL OCTOBER	1.4	±	0.1	79	1.1	1.6
	MODEL ANNUAL AVERAGE						
	Annual Threshold	1.2	±	0.1	79	1	1.4
	Persistent Threshold					0.8	2.1
BEAUFORT SEA	DATA	1.2	±	0.2	166	0.9	1.9
	MODEL OCTOBER	1.1	±	0.2	163	0.9	1.5
	MODEL ANNUAL AVERAGE						
	Annual Threshold	1	±	0.1	163	0.9	1.2
	Persistent Threshold					0.7	1.6
PACIFIC-ARCTIC REGION	DATA	1.4	±	0.2	384	0.9	2
	MODEL OCTOBER	1.4	±	0.3	354	0.9	2
	MODEL ANNUAL AVERAGE						
	Annual Threshold	1.2	±	0.2	354	0.9	1.5
	Persistent Threshold					0.7	2.1

The paradigm of Ω of more than 1.0 being good and less than 1.0 being bad for calcifying organisms is starting to break down as new research indicates that many species exhibit a wide range of responses to changing saturation states rather than absolute values or thresholds (e.g., Barton et al., 2012; Waldbusser et al., 2014). For example, pteropod shells have been observed to degrade in conditions of Ω_{arag} as high as 1.2 (Bednaršek et al., 2012, 2014), while other species are able to maintain calcification rates even below the saturation horizon (Long et al., 2013a,b). A better way of assessing the risk of changing carbonate chemistry across these shelf seas may be to estimate when conditions fall outside the range of present natural variability—that is, when organisms will be experiencing different conditions than those observed now. Outside this window we might assume that organisms will not have developed metabolic processes or responses designed to cope with these conditions. Under this scenario, areas with low natural variability and/or faster declines in Ω relative to present conditions will likely be more vulnerable than others. However, strong natural variability that produces periods of low Ω sufficient to force these organisms to adapt may indicate that some ecosystems are resilient to a wider range of Ω, and that much greater declines in Ω will be required to produce an impact on the ecosystems.

For the PAR shelves, the rate of decline in the annual average Ω_{arag} is similar among each of the shelf seas (~ -0.006 yr^{-1}; Table 2), but the overall magnitude of decline is slightly higher in the Bering Sea (~ -0.007 yr^{-1}; Table 2). Relative to the starting Ω_{arag} in 2012, the rate of decline by percent is also very similar among the shelf seas and this PAR model area ($\sim 5\%$ decade^{-1}; Table 2), with the percent decline slightly higher in the Beaufort Sea ($\sim 6\%$ decade^{-1}; Table 2). By rate alone, it does not appear that any one of these shelf seas is more vulnerable than the others. We then used these rates of decline to estimate when the
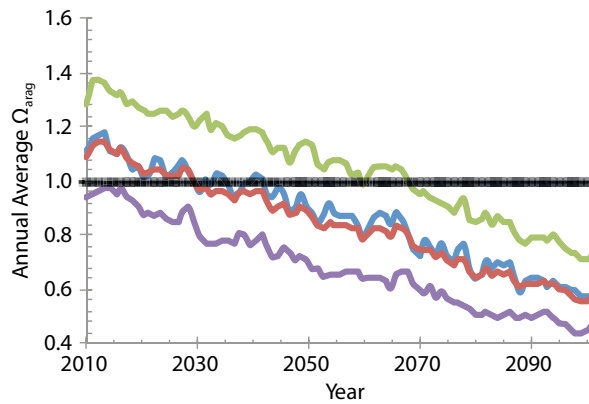

FIGURE 3. Time series of model-projected decline in the annual average Ω_{arag} for each basin and the whole shelf. The Bering Sea projection is shown in green, the Chukchi Sea in blue, and the Beaufort Sea in purple. The entire Pacific-Arctic Region average is shown in red. The saturation horizon ($\Omega = 1$) is indicated by a bold black line.
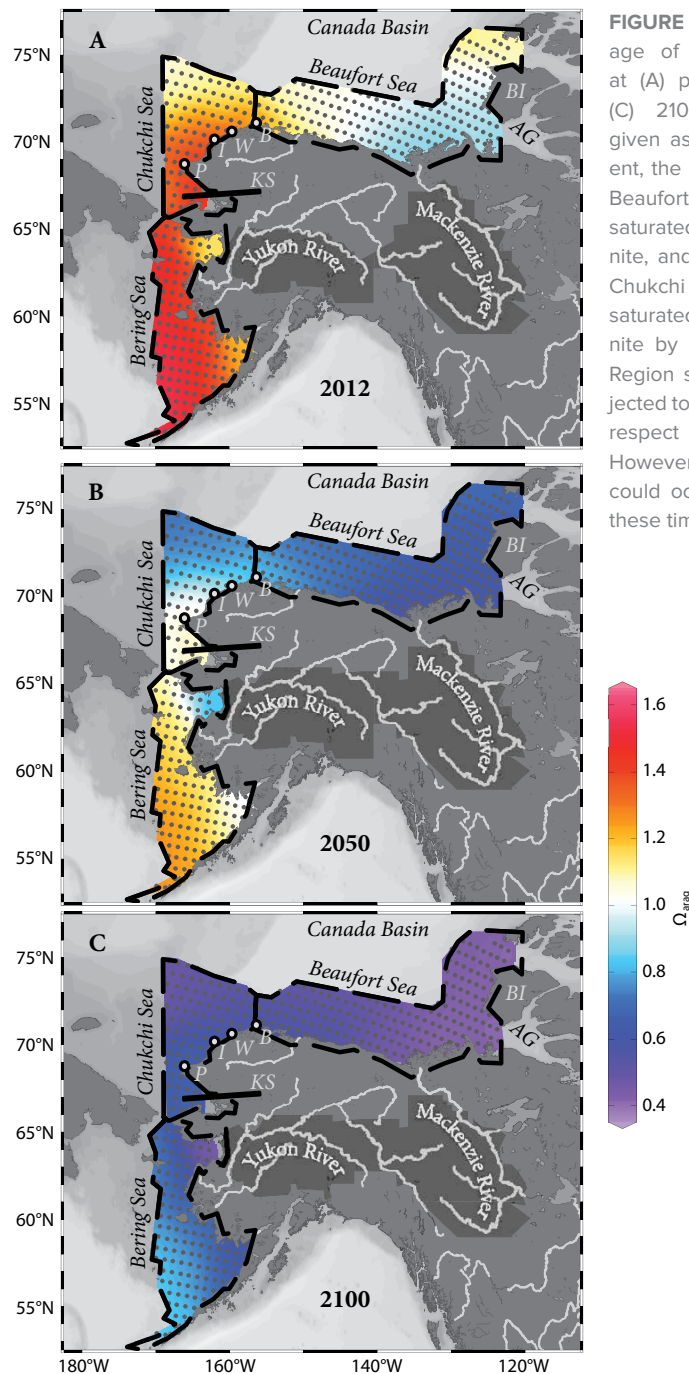

FIGURE 4. Annual average of model-simulated Ω_{arag} at (A) present, (B) 2050, and (C) 2100. Abbreviations are given as in Figure 1D. At present, the model projects that the Beaufort Sea is already undersaturated with respect to aragonite, and that the Beaufort and Chukchi Seas will both be undersaturated with respect to aragonite by 2050. All Pacific-Arctic Region surface waters are projected to be undersaturated with respect to aragonite by 2100. However, biological impacts could occur much sooner than these time frames (Table 3).

annual average saturation state for each of the shelf seas would pass outside of the range of present natural variability and defined two versions of this threshold for each area.

First, we described for each shelf sea when the spatially averaged annual saturation state passed below the minimum in the annual average Ω_{arag} for any grid cell in 2012 (annual threshold, Table 1). When the annual, shelf-wide average Ω_{arag} passes this first threshold, conditions over the entire shelf will be anomalous, or outside the window of present natural spatial variability, for most of the year, although the shelf-wide average Ω_{arag} may be inside this window during some months. In this case, the implication is that seasonal variability may create short periods of respite for the entire shelf from otherwise aberrantly low Ω_{arag} conditions. Second, we

also used these rates to predict when the spatially averaged annual Ω_{arag} passed below the minimum saturation state simulated in any grid cell during any month in 2012, or when the decline in Ω_{arag} will have overwhelmed even seasonal variability (persistent threshold; Table 1). When the annual, shelf-wide average saturation state passes this threshold, each shelf sea will experience near-perennial anomalous conditions relative to 2012. Seasonal variability may still create periods of respite from low Ω_{arag} conditions, but only in certain areas. When averaged spatially, the shelf sea will not experience any respite from these new, low Ω_{arag} conditions.

Table 3 gives the years that these thresholds are passed. The year that the undersaturation threshold for aragonite ($\Omega_{arag} < 1$) is reached is projected to

progress gradually upstream along the inflow path of Pacific waters at approximately 30-year intervals for the three PAR shelf regions. However, when considering natural seasonal variability, the Chukchi and the Beaufort Seas threshold crossing dates are much more similar to each other than to that of the Bering Sea. The "average" threshold, where conditions are mostly outside natural variability for most of the year, is passed in 2025 for the Beaufort Sea and 2027 for the Chukchi Sea, while the Bering Sea lags much further behind at 2044. The Persistent Thresholds, where conditions are mostly outside natural seasonal variability for all of the year, are passed ~30 years later for the Chukchi and Beaufort Seas, and ~40 years later for the Bering Sea.

This pattern surprisingly suggests that the Chukchi and Beaufort Seas are much more similar to each other and lower in variability than the Bering Sea, despite the similarities in the overall rate of saturation state decline (Table 2) and the range of variability in the model annual average (Table 1) across all three seas. This result likely stems from the difference between the minimum and the annual average Ω_{arag} for each shelf sea. Most of the conditions in the Bering Sea have a higher Ω_{arag} (see Figure 1), which raises the average Ω_{arag} relative to the total range. This means that a much greater decline is necessary in the Bering Sea to surpass these natural variability thresholds. Although the Bering and Chukchi Sea thresholds are crossed approximately 20–25 years apart, it is important to note that these areas do exhibit one key similarity that distinguishes both from the Beaufort Sea: the simulation projects that these two regions will pass the average threshold before passing the saturation horizon, indicating that impacts on the ecosystem may become apparent before the saturation horizon is reached. Even though some areas will not become persistently undersaturated in aragonite until 2100, many areas in the PAR will pass out of the range of natural variability for Ω_{arag} in the next few decades.

TABLE 2. Linear regression equations and rates of decline for the annual average model output. m indicates the slope, b the y-intercept, and r² indicates the square of the correlation coefficient. The last column indicates the percent decline from the annual average in 2012 across one decade.

	m	b	r²	% 10 yr⁻¹
Bering Sea	−0.007	15.3	0.98	−4.91
Chukchi Sea	−0.006	13.7	0.96	−5.13
Beaufort Sea	−0.006	12.6	0.97	−5.89
Continental Shelf	−0.006	13.7	0.98	−5.34

TABLE 3. Years when the annual average Ω_{arag} will reach important biological thresholds. Included here are the years when average annual conditions reach the saturation horizon, the thermodynamic value when dissolution of mineral structures is favored (Saturation Threshold); the year when the annual average Ω_{arag} declines below the average 2012 minimum (Annual Threshold), although seasonally there may be some respite from these new, low-Ω_{arag} conditions for the shelf as a whole; and the year when the annual average Ω_{arag} declines below the minimum observed across all monthly outputs for 2012, when these new, low-Ω_{arag} conditions are perennial for the entire year over most of the shelf (Persistent Threshold). The bounds for the Annual and Persistent Thresholds for each basin and the entire Pacific-Arctic Region are indicated in Table 1. Note that for the Beaufort Sea, the model indicates that the undersaturation threshold has already been passed at present, and that the Annual Threshold for the Beaufort and Chukchi Seas will approach in the next 12 years. Projections based solely on observed data and trends indicate that thresholds will be passed half as quickly, adding over 80 years to these time frames in some cases.

	Saturation Threshold Ω < 1	Annual Threshold Ω < Ann Min	Persistent Threshold Ω < Mo Min
Bering Sea	2062	2044	2085
Chukchi Sea	2033	2027	2059
Beaufort Sea	2001	2025	2054
Pacific-Arctic Region	2030	2052	2079

This first approximation highlights the impending stresses that the ecosystems of these shelf seas may soon experience. However, we have used an intercomparison between CESM and data from only one observation program that spans only one month out of the year. Even in this comparison, the extreme spatial variability and fine-scale features we identified show that it will be difficult, if not impossible, to quantify transitions in biogeochemical conditions over the next few decades without well-calibrated models. The next step in this process should be an intensive effort to synthesize all of the currently available observation data from the PAR and use it to fully validate model results and address the parameterization of the Yukon and Mackenzie Rivers in CESM. This effort would improve the model forecasting ability and allow for more precise estimates of when biogeochemical thresholds will be crossed, and when biological impacts may manifest.

CONCLUSIONS

The high-latitude oceans of the PAR have naturally low CO_3^{2-} concentrations and are considered to be more vulnerable to the impacts of OA on shorter time scales than lower latitude oceans because additional losses of CO_3^{2-} from OA represent much greater proportional changes to their systems. Here, we have used data collected over broad spatial scales in October 2011 and 2012 and compared them to outputs from the CESM1(BGC) ocean simulations. We found that the model outputs closely matched our observed data except in cases where river water dominated on the continental shelves, mainly at the outflow of the Yukon and Mackenzie Rivers. Although unique biogeochemical interactions control carbonate mineral saturation states and therefore the extent, duration, and intensity of OA events in each shelf sea of the PAR, the model captured the seasonal and spatial variability at a resolution that can be used for generating future trends in Ω_{arag}.

We used the model to project future Ω_{arag} (Figure 4) based on the RCP 8.5 CO_2 emission scenario and found that the critical saturation threshold for each shelf sea and even for the PAR as a whole will be passed prior to 2079. Despite some short respites from low-Ω_{arag} conditions, annual average conditions passed outside of natural variability (crossed the annual threshold) in 2025 for the Beaufort Sea and 2027 for the Chukchi Sea, while the Bering Sea lags further behind at 2044. Approximately 30 years later for the Chukchi and Beaufort Seas and ~40 years later for the Bering Sea, seasonal peaks in average Ω_{arag} were overwhelmed by increasing OA (crossed the persistent threshold), resulting in near-perennial conditions outside of natural variability.

While it is still unclear what ultimate biological impacts will result from these biogeochemical changes, it is probably safe to assume that they will have detrimental effects on ecosystems that are already under pressure from rising temperatures and other climate-driven stressors. Like in the Southern Ocean, pteropods are expected to play an important, if not critical, role in high-latitude food webs, and these organisms have already been shown to be impacted by conditions similar to those in the PAR (Bednaršek et al., 2012). Shifts in biological communities are occurring rapidly as a result of OA. Continued monitoring and model development in the PAR is essential to understanding the ecosystem transitions currently underway due to the suite of anthropogenically induced pressures. This region provides unique insights into how the global ocean will respond to human activities, and it is our best hope for developing the understanding that will be needed to mitigate and adapt to what will be our new, modern ocean environment. 🌀

REFERENCES

Anderson, L.G., and S. Kaltin. 2001. Carbon fluxes in the Arctic Ocean: Potential impact by climate change. *Polar Research* 20:225–232, http://dx.doi.org/10.1111/j.1751-8369.2001.tb00060.x.

Arrigo, K.R., and G.L. van Dijken. 2011. Secular trends in Arctic Ocean net primary production. *Journal of Geophysical Research* 116, C09011, http://dx.doi.org/10.1029/2011JC007151.

Arrigo, K.R., G. van Dijken, and S. Pabi. 2008. Impact of a shrinking Arctic ice cover on marine primary production. *Geophysical Research Letters* 35, L19603, http://dx.doi.org/10.1029/2008GL035028.

Barry, J.P., S. Widdicombe, and J.M. Hall-Spenser. 2011. Effects of ocean acidification on marine biodiversity and ecosystem function in ocean acidification. Pp. 192–209 in *Ocean Acidification*. J.-P. Gattuso and L. Hansson, eds, Oxford University Press, Oxford.

Barton, A., B. Hales, G. Waldbusser, C. Langdon, and R.A. Feely. 2012. The Pacific oyster, *Crassostrea gigas*, shows negative correlation to naturally elevated carbon dioxide levels: Implications for near-term ocean acidification effects. *Limnology and Oceanography* 57:698–710, http://dx.doi.org/10.4319/lo.2012.57.3.0698.

Bates, N.R., W.-J. Cai, and J.T. Mathis. 2011. The ocean carbon cycle in the western Arctic Ocean: Distributions and air-sea fluxes of carbon dioxide. *Oceanography* 24(3):186–201, http://dx.doi.org/10.5670/oceanog.2011.71.

Bates, N.R., R. Garley, K.E. Frey, K.L. Shake, and J.T. Mathis. 2014. Sea-ice melt CO_2-carbonate chemistry in the western Arctic Ocean: Meltwater contributions to air-sea CO_2 gas exchange, mixed layer properties and rates of net community production under sea ice. *Biogeosciences Discussions* 11:1,097–1,145, http://dx.doi.org/10.5194/bgd-11-1097-2014.

Bates, N.R., and J.T. Mathis. 2009. The Arctic Ocean marine carbon cycle: Evaluation of air-sea CO_2 exchanges, ocean acidification impacts and potential feedbacks. *Biogeosciences* 6:2,433–2,459, http://www.biogeosciences.net/6/2433/2009/bg-6-2433-2009.pdf

Bednaršek, N., R.A. Feely, J.C.P. Reum, W. Peterson, J. Menkel, S.R. Alin, and B. Hales 2014. *Limacina helicina* shell dissolution as an indicator of declining habitat suitability due to ocean acidification in the California Current Ecosystem. *Proceedings of the Royal Society B* 281, 20140123, http://dx.doi.org/10.1098/rspb.2014.0123.

Bednaršek, N., G.A. Tarling, D.C.E. Bakker, S. Fielding, E.M. Jones, H.J. Venables, P. Ward, A. Kuzirian, B. Lézé, R.A. Feely, and E.J. Murphy 2012. Extensive dissolution of live pteropods in the Southern Ocean. *Nature Geoscience* 5:881–885, http://dx.doi.org/10.1038/ngeo1635.

Bell, G., and A. Gonzalez. 2009. Evolutionary rescue can prevent extinction following environmental change. *Ecology Letters* 12:942–948, http://dx.doi.org/10.1111/j.1461-0248.2009.01350.x.

Bernhardt, J.R., and H.M. Leslie. 2013. Resilience to climate change in coastal marine ecosystems. *Annual Review of Marine Science* 5:371–392, http://dx.doi.org/10.1146/annurev-marine-121211-172411.

Byrne, R.H., S. Mecking, R.A. Feely, and X. Liu. 2010. Direct observations of basin-wide acidification of the North Pacific Ocean. *Geophysical Research Letters* 37, L02601, http://dx.doi.org/10.1029/2009GL040999.

Cai, W.-J., L. Chen, B. Chen, Z. Gao, S.H. Lee, J. Chen, D. Pierrot, K. Sullivan, Y. Wang, X. Hu, and others. 2010. Decrease in the CO_2 uptake capacity in an ice-free Arctic Ocean basin. *Science* 329:556–559, http://dx.doi.org/10.1126/science.1189338.

Caldeira, K., and M.E. Wickett. 2003. Anthropogenic carbon and ocean pH. *Nature* 425:365, http://dx.doi.org/10.1038/425365a.

Carmack, E., and P. Wassmann. 2006. Food webs and physical-biological coupling on pan-Arctic shelves: Unifying concepts and comprehensive perspectives. *Progress in Oceanography* 71:446–477, http://dx.doi.org/10.1016/j.pocean.2006.10.004.

Comiso, J.C., C.L. Parkinson, R. Gersten, and L. Stock. 2008. Accelerated decline in the Arctic sea ice cover. *Geophysical Research Letters* 3, L01703, http://dx.doi.org/10.1029/2007GL031972.

Cooley, S.R., and S.C. Doney. 2009. Anticipating ocean acidification's economic consequences for commercial fisheries. *Environmental Research Letters* 4:024007, http://dx.doi.org/10.1088/1748-9326/4/2/024007.

Cooley, S.R., N. Lucey, H. Kite-Powell, and S.C. Doney. 2012. Nutrition and income from molluscs today imply vulnerability to ocean acidification tomorrow. *Fish and Fisheries* 13:182–215, http://dx.doi.org/10.1111/j.1467-2979.2011.00424.x.

Cross, J.N., J.T. Mathis, and N.R. Bates. 2012. Hydrographic controls on net community production and total organic carbon distributions in the eastern Bering Sea. *Deep Sea Research Part II* 65–70:98–109, http://dx.doi.org/10.1016/j.dsr2.2012.02.003.

Cross, J.N., J.T. Mathis, N.R. Bates, and R.H. Byrne. 2013. Conservative and non-conservative variations of total alkalinity on the southeastern Bering Sea shelf. *Marine Chemistry* 154:100–112, http://dx.doi.org/10.1016/j.marchem.2013.05.012.

Cross, J.N., J.T. Mathis, M.W. Lomas, S.B. Moran, M.S. Baumann, D. Shull, C.W. Mordy, M.L. Ostendorf, N.R. Bates, P.J. Stabeno, and J.M. Grebmeier. 2014. Integrated assessment of the carbon budget in the southeastern Bering Sea. *Deep Sea Research Part II* 109:112–124, http://dx.doi.org/10.1016/j.dsr2.2014.03.003.

Dickson, A.G. 1990. Thermodynamics of the dissociation of boric acid in synthetic seawater from 273.15 to 318.15 K. *Deep Sea Research Part A* 37:755–766, http://dx.doi.org/10.1016/0198-0149(90)90004-F.

Dickson, A.G., and C. Goyet, eds. 1994. *Handbook of Methods for the Analysis of Various Parameters of the Carbon Dioxide System in Seawater, Version 2.0*. Rep. ORNL/CDIAC-74, US Department of Energy, Washington, DC.

Dickson, A.G., and F.J. Millero. 1987. A comparison of the equilibrium constants for the dissociation of carbonic acid in seawater media. *Deep Sea Research Part A* 34:1,733–1,743, http://dx.doi.org/10.1016/0198-0149(87)90021-5.

Evans, W., and J.T. Mathis. 2013. The Gulf of Alaska coastal ocean as an atmospheric CO_2 sink. *Continental Shelf Research* 65:52–63, http://dx.doi.org/10.1016/j.csr.2013.06.013.

Evans, W., J.T. Mathis, and J.N. Cross. 2014. Calcium carbonate corrosivity in an Alaskan inland sea. *Biogeosciences* 11:365–379, http://dx.doi.org/10.5194/bg-11-365-2014.

Fabry, V.J., J.B. McClintock, J.T. Mathis, and J.M. Grebmeier. 2009. Ocean acidification at high latitudes: The bellwether. *Oceanography* 22(4):160–171, http://dx.doi.org/10.5670/oceanog.2009.105.

Feely, R.A., S.C. Doney, and S.R. Cooley. 2009. Ocean acidification: Present conditions and future changes in a high-CO_2 world. *Oceanography* 22(4):36–47, http://dx.doi.org/10.5670/oceanog.2009.95.

Feely, R.A., C.L. Sabine, K. Lee, W. Berelson, J. Kleypas, V.J. Fabry, and F.J. Millero. 2004. Impact of anthropogenic CO_2 on the $CaCO_3$ system in the oceans. *Science* 305:362–366, http://dx.doi.org/10.1126/science.1097329.

Frisch, L.C., J.T. Mathis, N.P. Kettle, and S.F. Trainor. 2015. Gauging perceptions of ocean acidification in Alaska. *Marine Policy* 53:101–110, http://dx.doi.org/10.1016/j.marpol.2014.11.022.

Garneau, M.E., W.F. Vincent, R. Terrado, and C. Lovejoy. 2009. Importance of particle-associated bacterial heterotrophy in a coastal Arctic ecosystem. *Journal of Marine Systems* 75:185–197, http://dx.doi.org/10.1016/j.jmarsys.2008.09.002.

Hoffman, R.R., and C.M. Sgrò. 2011. Climate change and evolutionary adaptation. *Nature* 470:479–485, http://dx.doi.org/10.1038/nature09670.

Hönisch, B., A. Ridgwell, D.N. Schmidt, E. Thomas, S.J. Gibbs, A. Sluijs, R. Zeebe, L. Kump, R.C. Martindale, S.E. Greene, and others. 2012. The geological record of ocean acidification. *Science* 335:1,058–1,063, http://dx.doi.org/10.1126/science.1208277.

Hunt, G.L. Jr., K.O. Coyle, L.B. Eisner, E.V. Farley, R.A. Heintz, F. Mueter, J.M. Napp, J.E. Overland, P.H. Ressler, S. Salo, and P.J. Stabeno. 2011. Climate impacts on eastern Bering Sea foodwebs: A synthesis of new data and an assessment of the Oscillating Control Hypothesis. *ICES Journal of Marine Science* 68:1,230–1,243, http://dx.doi.org/10.1093/icesjms/fsr036.

Kadko, D., R.S. Pickart, and J.T. Mathis. 2008. Age characteristics of a shelf-break eddy in the western Arctic and implications for shelf-basin exchange. *Journal of Geophysical Research* 113, C02018, http://dx.doi.org/10.1029/2007JC004429.

Keppel-Aleks, G., J.T. Randerson, K. Lindsay, B.B. Stephens, J.K. Moore, S.C. Doney, P.E. Thornton, N.M. Mahowald, F.M. Hoffman, C. Sweeney, and others. 2013. Atmospheric carbon dioxide variability in the Community Earth System Model: Evaluation and transient dynamics during the twentieth and twenty-first centuries. *Journal of Climate* 26:4,447–4,475, http://dx.doi.org/10.1175/JCLI-D-12-00589.1.

Key, R.M., A. Kozyr, C.L. Sabine, K. Lee, R. Wanninkhof, J.L. Bullister, R.A. Feely, F.J. Millero, and T.-H. Peng. 2004. A global ocean carbon climatology: Results from Global Data Analysis Project (GLODAP). *Global Biogeochemical Cycles* 18, GB4031, http://dx.doi.org/10.1029/2004GB002247.

Kroeker, K.J., R.L. Kordas, R.N. Crim, and G.G. Singh. 2010. Meta-analysis reveals negative yet variable effects of ocean acidification on marine organisms. *Ecology Letters* 13:1,419–1,434, http://dx.doi.org/10.1111/j.1461-0248.2010.01518.x.

Lavoie, D., K.L. Denman, and R.W. Macdonald. 2010. Effects of future climate change on primary productivity and export fluxes in the Beaufort Sea. *Journal of Geophysical Research* 115, C04018, http://dx.doi.org/10.1029/2009JC005493.

Lee, H., S.C. Swenson, A.G. Slater, and D.M. Lawrence. 2014. Effects of excess ground ice on projections of permafrost in a warming climate. *Environmental Research Letters* 9:124006, http://dx.doi.org/10.1088/1748-9326/9/12/124006.

Lewis, E.R., and D.W.R. Wallace. 1995. *Basic Programs for the CO_2 System in Seawater*. Rep. BNL-61827, Brookhaven National Laboratory, Upton, NY.

Lindsay, K., G.B. Bonan, S.C Doney, F.M. Hoffmann, D.M. Lawrence, M.C. Long, N.M. Mahowald, J.K. Moore, J.T. Randerson, and P.E. Thornton. 2014. Preindustrial-control and twentieth-century carbon cycle experiments with the earth system model CESM1(BGC). *Journal of Climate* 27:8,981–9,005, http://dx.doi.org/10.1175/JCLI-D-12-00565.1.

Long, M.C., K. Lindsay, and S. Peacock. 2013. Twentieth-century oceanic carbon uptake and storage in CESMI(BGC). *Journal of Climate* 26(18):6,775–6,800, http://dx.doi.org/10.1175/JCLI-D-12-00184.1.

Long, W.C., K.M. Swiney, and R.J. Foy. 2013a. Effects of ocean acidification on the embryos and larvae of red king crab, *Paralithodes camtschaticus*. *Marine Pollution Bulletin* 69:38–47, http://dx.doi.org/10.1016/j.marpolbul.2013.01.011.

Long, W.C., K.M. Swiney, C. Harris, H.N. Page, and R.J. Foy. 2013b. Effects of ocean acidification on juvenile red king crab (*Paralithodes camtschaticus*) and Tanner crab (*Chionoecetes bairdi*) growth, condition, calcification, and survival. *PLoS ONE* 8(4):e60959, http://dx.doi.org/10.1371/journal.pone.0060959.

Macdonald, R.W., L.G. Anderson, J.P. Christensen, L.A. Miller, I.P. Semiletov, and R. Stein. 2010. Polar margins: The Arctic Ocean. Pp. 291–303 in *Carbon and Nutrient Fluxes in Continental Margins: A Global Synthesis*. K.K. Liu, L. Atkinson, R. Quiñones, and L. Talaue-McManus, eds, Springer, NY.

Mathis, J.T., N.R. Bates, D.A. Hansell, and T. Babila. 2009. Net community production in the northeastern Chukchi Sea. *Deep Sea Research Part II* 56:1,213–1,222, http://dx.doi.org/10.1016/j.dsr2.2008.10.017.

Mathis, J.T., R.H. Byrne, C.L. McNeil, R.P. Pickart, L. Juranek, S. Liu, J. Ma, R.A. Easley, M.W. Elliot, J.N. Cross, and others. 2012. Storm-induced upwelling of high $p$$CO_2$ waters onto the continental shelf of the western Arctic Ocean and implications for carbonate mineral saturation states. *Geophysical Research Letters* 39, L07606, http://dx.doi.org/10.1029/2012GL051574.

Mathis, J.T., S.R. Cooley, N. Lucey, S. Colt, J. Ekstrom, T. Hurst, C. Hauri, W. Evans, J.N. Cross, and R.A. Feely. In press. Ocean acidification risk assessment for Alaska's fishery sector. *Progress in Oceanography*, http://dx.doi.org/10.1016/j.pocean.2014.07.001.

Mathis, J.T., J.N. Cross, and N.R. Bates. 2011a. The role of ocean acidification in systemic carbonate mineral suppression in the Bering Sea. *Geophysical Research Letters* 38, L19602, http://dx.doi.org/10.1029/2011GL048884.

Mathis, J.T., J.N. Cross, and N.R. Bates. 2011b. Coupling primary production and terrestrial runoff to ocean acidification and carbonate mineral suppression in the eastern Bering Sea. *Journal of Geophysical Research* 116, C02030, http://dx.doi.org/10.1029/2010JC006453.

Mathis, J.T., R.S. Pickart, D.A. Hansell, D. Kadko, and N.R. Bates. 2007. Eddy transport of organic carbon and nutrients from the Chukchi Shelf: Impact on the upper halocline of the western Arctic Ocean. *Journal of Geophysical Research* 112, C05011, http://dx.doi.org/10.1029/2006JC003899.

Mathis, J.T., and J.M. Questel. 2013. Assessing seasonal changes in carbonate parameters across small spatial gradients in the Northeastern Chukchi Sea. *Continental Shelf Research* 67:42–51, http://dx.doi.org/10.1016/j.csr.2013.04.041.

Mehrbach, C., C.H. Culberson, J.E. Hawley, and R.M. Pytkowitz. 1973. Measurement of the apparent dissociation constants of carbonic

acid in seawater at atmospheric pressure. *Limnology and Oceanography* 18:897–907, http://dx.doi.org/10.4319/lo.1973.18.6.0897.

Orr, J.C. 2011. Recent and future changes in ocean carbonate chemistry. Pp. 41–66 in *Ocean Acidification*. J.-P. Gattuso and L. Hansson, eds, Oxford University Press, Oxford, UK.

Orr, J.C., V.J. Fabry, O. Aumont, L. Bopp, S.C. Doney, R.A. Feely, A. Gnanadesikan, N. Gruber, A. Ishida, F. Joos, and others. 2005. Anthropogenic ocean acidification over the twenty-first century and its impact on calcifying organisms. *Nature* 437:681–686, http://dx.doi.org/10.1038/nature04095.

Peterson, B.J., R.M. Holmes, J.W. McClelland, C.J. Vörösmarty, R.B. Lammers, A.I. Shiklomanov, I.A. Shiklomanov, and S. Rahmstorf. 2002. Increasing river discharge to the Arctic Ocean. *Science* 298:2,171–2,173, http://dx.doi.org/10.1126/science.1077445.

Reisdorph, S.C., and J.T. Mathis. 2014. The dynamic controls on carbonate mineral saturation states and ocean acidification in a glacially dominated estuary. *Estuarine, Coastal and Shelf Science* 144:8–18, http://dx.doi.org/10.1016/j.ecss.2014.03.018.

Roy, T., L. Bopp, M. Gehlen, B. Schneider, P. Cadule, T.L. Frölicher, J. Segschneider, J. Tjiputra, C. Heinze, and F. Joos. 2011. Regional impacts of climate change and atmospheric CO_2 on future ocean carbon uptake: A multimodel linear feedback analysis. *Journal of Climate* 24:2,300–2,318, http://dx.doi.org/10.1175/2010JCLI3787.1.

Sabine, C.L., and R.A. Feely. 2007. The oceanic sink for carbon dioxide. Pp. 31–49 in *Greenhouse Gas Sinks*. D. Reay, N. Hewitt, J. Grace, and K. Smith, eds, CABI Publishing, Oxfordshire, UK.

Sabine, C.L., R.A. Feely, N. Gruber, R.M. Key, K. Lee, J.L. Bullister, R. Wanninkhof, C.S. Wong, D.W.R. Wallace, B. Tilbrook, and others. 2004. The oceanic sink for anthropogenic CO_2. *Science* 305:367–371, http://dx.doi.org/10.1126/science.1097403.

Stabeno, P.J., E.V. Farley Jr., N.B. Kachel, S. Moore, C.W. Mordy, J.M. Napp, J.E. Overland, A.I. Pinchuk, and M.F. Sigler. 2012a. A comparison of the physics of the northern and southern shelves of the eastern Bering Sea and some implications for the ecosystem. *Deep Sea Research Part II* 65–70:14–30, http://dx.doi.org/10.1016/j.dsr2.2012.02.019.

Stabeno, P.J., N.B. Kachel, S.E. Moore, J.M. Napp, M. Sigler, A. Yamaguchi, and A.N. Zerbini. 2012b. Comparison of warm and cold years on the southeastern Bering Sea shelf and some implications for the ecosystem. *Deep Sea Research Part II* 65–70:31–45, http://dx.doi.org/10.1016/j.dsr2.2012.02.020.

Steinacher, M., F. Joos, T.L. Frölicher, G.-K. Platter, and S.C. Doney. 2009. Imminent ocean acidification in the Arctic projected with the NCAR global coupled carbon cycle-climate model. *Biogeosciences* 6:515–533, http://dx.doi.org/10.5194/bg-6-515-2009.

Striegl, R.G., M.M. Dornblaser, G.R. Aiken, K.P. Wickland, and P.A. Raymond. 2007. Carbon export and cycling by the Yukon, Tanana, and Porcupine rivers, Alaska, 2001–2005. *Water Resources Research* 43, WO2411, http://dx.doi.org/10.1029/2006WR005201.

Stroeve, J., M.M. Holland, W. Meier, T. Scambos, and M. Serreze. 2007. Arctic sea ice decline: Faster than forecast. *Geophysical Research Letters* 34, L09501, http://dx.doi.org/10.1029/2007GL029703.

van Vuuren, D.P., J. Edmonds, M. Kainuma, K. Riahi, A. Thomson, K. Hibbard, G.C. Hurtt, T. Kram, V. Krey, J.-F. Lamarque, and others. 2011. The representative concentration pathways: An overview. *Climatic Change* 109:5–31, http://dx.doi.org/10.1007/s10584-011-0148-z.

Waldbusser, G.G., B. Hales, C.J. Langdon, B.A. Haley, P. Schrader, E.L. Brunner, M.W. Gray, C.A. Miller, and I. Gimenez. 2014. Saturation-state sensitivity of marine bivalve larvae to ocean acidification. *Nature Climate Change* 5:273–280, http://dx.doi.org/10.1038/nclimate2479.

Walvoord, M.A., and R.G. Striegl. 2007. Increased groundwater to stream discharge from permafrost thawing in the Yukon River basin: Potential impacts on lateral export of carbon and nitrogen. *Geophysical Research Letters* 34, L12402, http://dx.doi.org/10.1029/2007GL030216.

Weiss, R.F. 1974. Carbon dioxide in water and seawater: The solubility of a non-ideal gas. *Marine Chemistry* 2:203–215, http://dx.doi.org/10.1016/0304-4203(74)90015-2.

Willi, Y., J. Van Buskirk, and A.A. Hoffman. 2006. Limits to the adaptive potential of small populations. *Annual Reviews of Ecology, Evolution and Systematics* 37:433–458, http://dx.doi.org/10.1146/annurev.ecolsys.37.091305.110145.

Yamamoto-Kawai, M., F. McLaughlin, and E. Carmack. 2013. Ocean acidification in the three oceans surrounding northern North America. *Journal of Geophysical Research* 118:6,274–6,284, http://dx.doi.org/10.1002/2013JC009157.

Yamamoto-Kawai, M., F.A. McLaughlin, E.C. Carmack, S. Nishino, and K. Shimada. 2009a. Aragonite undersaturation in the Arctic Ocean: Effects of ocean acidification and sea ice melt. *Science* 326:1,098–1,100, http://dx.doi.org/10.1126/science.1174190.

Yamamoto-Kawai, M., F.A. McLaughlin, E.C. Carmack, S. Nishino, K. Shimada, and N. Kurita. 2009b. Surface freshening of the Canada Basin, 2003–2007: River runoff versus sea ice meltwater. *Journal of Geophysical Research* 114, C00A05, http://dx.doi.org/10.1029/2008JC005000.

AUTHORS. **Jeremy T. Mathis** (jeremy.mathis@noaa.gov) is Supervisory Oceanographer, National Oceanic and Atmospheric Administration (NOAA), Pacific Marine Environmental Laboratory (PMEL), Seattle, WA, USA, and Affiliate Professor, Ocean Acidification Research Center, School of Fisheries and Ocean Sciences, University of Alaska Fairbanks, Fairbanks, AK, USA. **Jessica N. Cross** is Postdoctoral Fellow, NOAA, PMEL, Seattle, WA, USA, and the Ocean Acidification Research Center, School of Fisheries and Ocean Sciences, University of Alaska Fairbanks, Fairbanks, AK, USA. **Wiley Evans** is Research Associate, NOAA, PMEL, Seattle, WA, USA, and Ocean Acidification Research Center, School of Fisheries and Ocean Sciences, University of Alaska Fairbanks, Fairbanks, AK, USA. **Scott C. Doney** is Chair, Department of Marine Chemistry and Geochemistry, Woods Hole Oceanographic Institution, Woods Hole, MA, USA.